(Received 31 May 2024, Accepted 22 July 2024, Scheduled 2 August 2024)

Adaptive Cross Approximation Accelerates Compressive Sensing-Based Method of Moments for Solving Electromagnetic Scattering Problems

Dai Dong[1], Zhonggen Wang[1], Wenyan Nie[2,*], Fei Guo[1], Yufa Sun[3], Pan Wan[3], and Chenlu Li[4]

[1]*School of Electrical and Information Engineering, Anhui University of Science and Technology, Huainan 232001, China*
[2]*School of Mechanical and Electrical Engineering, Huainan Normal University, Huainan 232001, China*
[3]*School of Electronics and Information Engineering, Anhui University, Hefei 230061, China*
[4]*School Electrical and Information Engineering, Hefei Normal University, Hefei 230061, China*

ABSTRACT: In this paper, a novel measurement matrix construction method based on adaptive cross-approximation (ACA) is proposed to improve the performance of the compressive sensing-based method of moments (CS-MoM) for analyzing electromagnetic scattering problems. ACA is based on a weight scheme and is able to recognize the rows and columns that contribute significantly to the matrix. Thus, the object is divided into multiple blocks, and the impedance matrix is partitioned into near-field and far-field groups to establish the condition for applying ACA. Then, the row indexes are extracted from the group with the highest number of ACA recognized rows in the far-field groups of each block. Finally, by combining all row indexes to extract the impedance matrix, a lower-dimensional and deterministic measurement matrix is constructed, thereby improving computational efficiency. Numerical simulation results validate the accuracy and effectiveness of the proposed method.

1. INTRODUCTION

The method of moments (MoM) [1, 2] is widely used in the numerical calculation of electromagnetic fields and is regarded as an evaluation standard. However, the computational complexity of solving matrix equation in the electrically large problems is relatively high. To alleviate this problem, various fast algorithms have been proposed to accelerate the matrix vector products (MVPs), such as fast multipole method (FMM) [3] and multilevel FMM (MLFMM) [4]. Another approach is using macro basis functions to reduce the number of unknowns to achieve matrix dimensionality reduction, and the most typical one is the characteristic basis function method (CBFM) [5, 6]. However, the construction of reduced matrix involves numerous matrix-vector products, and its construction process is time-consuming.

In recent years, compressive sensing (CS) [7, 8] technique has been introduced into MoM to reduce computational complexity, called CS-based MoM (CS-MoM), providing a new scheme to solve the above problems. Depending on the difference in solving the problem, CS-MoM has formed two computational models. One is novel excitation source model [9–11], and the other is underdetermined equation model [12, 13]. The former achieves efficient handling of monostatic problems by compressing the number of excitations and decreasing the number of equations to be solved. In contrast, the latter changes the algorithmic structure of MoM by transforming the matrix equation into an underdetermined equation, which is suitable for solving bistatic problems.

The CS theory states that the signals can be recovered from significantly fewer measurements than the original data. The above properties indicate that constructing a well-performing measurement matrix will have a positive impact on the computational results. However, in the latter computational model, the measurement matrix is commonly constructed by left-multiplied Gaussian matrix [14] or randomly extracting certain rows of the impedance matrix [15], and such randomness leads to uncertain calculation results. Therefore, Gao et al. analyzed the irrationality of constructing the measurement matrix by randomly extracting the impedance matrix and proposed a novel CS-MoM (NCS-MoM) [16], which uses uniform extraction instead of random extraction. While NCS-MoM analyzes the formation of the measurement matrix from the perspective of the impedance matrix's structure, uniform extraction is just a simple sampling strategy and does not guarantee obtaining the optimal measurement matrix. Considering that NCS-MoM uses the Rao-Wilton-Glisson (RWG) [17] basis functions as test functions, and each test function corresponds one-to-one with the rows of the impedance matrix. However, whether through random extraction or uniform extraction, neither method can recognize the test functions that contribute significantly to accuracy. Therefore, a method capable of recognizing these test functions and delivering reliable accuracy is highly necessary. Besides, the induced currents are normally non-sparse and need to be sparsely transformed.

* Corresponding author: Wenyan Nie (wynie5240@163.com).

Up to now, the characteristic basis functions (CBFs) [18, 19], characteristic modes (CMs), [20] and Krylov subspace [21, 22] are applicable as sparse basis for analyzing three dimensional (3D) problems. Taking into account that the construction of basis functions is independent of the excitations and benefits from the domain decomposition method, the CMs are more suitable for analyzing the electrically large problems.

Different from previous works, to further enhance the performance of CS-MoM, an adaptive cross approximation (ACA) based CS-MoM is proposed, called ACA-CS-MoM. Because each test function has a different impact on accuracy, we introduce the purely mathematical method ACA [23, 24] to recognize the test functions contributing significantly to accuracy. Thus, ACA-CS-MoM requires fewer observations to obtain precise solution. Compared with the strategies of random extraction and uniform extraction, the use of the row indexes obtained via ACA to extract the impedance matrix for constructing the measurement matrix is more convincing. Furthermore, adjusting the threshold of ACA can control the number of rows in the measurement matrix, making it possible to reduce time costs by selecting an appropriate threshold. Meanwhile, the least squares [25] is applied as the reconstruction algorithm to solve the current coefficients. Due to the lower dimensionality of the measurement matrix of the proposed method, it is more efficient in both matrix construction and the solution of the overdetermined equation.

The rest of this paper is organized as follows. In Section 2, the theoretical content of compressive sensing and the proposed method is presented. In Section 3, the complexity analysis of several methods is given. In Section 4, the effectiveness of the ACA-CS-MoM is evaluated through numerical simulations. Finally, the conclusion is given in Section 5.

2. THEORY

2.1. Conventional CS-MoM

For the electromagnetic scattering problems of perfect electrical conductor (PEC) objects, the MoM applies the RWG basis functions to transform the electric field integral equation (EFIE) into a matrix equation:

$$\mathbf{ZI} = \mathbf{V}, \tag{1}$$

where $\mathbf{Z}$ denotes a full rank impedance matrix of size $N \times N$, and N is the number of unknowns. $\mathbf{I}$ and $\mathbf{V}$ denote the current vector and excitation vector, respectively. The elements of $\mathbf{Z}$ and $\mathbf{V}$ can be expressed as follows [2]:

$$z_{mn} = jk\eta \int_S \int_{S'} G\left(f_m \cdot f_n - \frac{1}{k^2} \nabla \cdot f_m \nabla' \cdot f_n\right) dS' dS, \tag{2}$$

$$v_m = \int_S f_m \cdot \mathbf{V}^i dS, \tag{3}$$

where k, η, and G denote the wavenumber, wave impedance, and Green's function, respectively. f_m is the mth RWG basis function, and $\mathbf{V}^i$ is the incident wave. Obviously, the calculation of the impedance elements involves extensive Green's function factors and integration operations, which are quite time-consuming.

Fortunately, the introduction of the CS technique decreases the number of rows filled in the impedance matrix, while avoiding the complex matrix product operations in the reduced matrix construction, resulting in a more efficient solution. In CS-MoM, there are three main components: measurement, sparsity, and reconstruction.

To begin with, CS-MoM establishes the underdetermined equation by randomly extracting certain rows of $\mathbf{Z}$ and $\mathbf{V}$ as measurement matrix $\tilde{\mathbf{Z}}$ and measurement value $\tilde{\mathbf{V}}$:

$$\tilde{\mathbf{Z}}\mathbf{I} = \tilde{\mathbf{V}}. \tag{4}$$

Recently, a new measurement matrix construction method has been proposed [16], which forms a deterministic measurement matrix by uniformly extracting the impedance matrix. The schematic diagram of randomly extracted and uniformly extracted impedance matrix is shown in Figure 1.

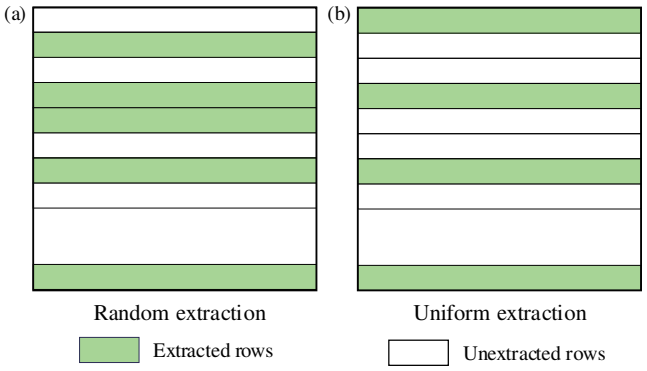

FIGURE 1. Schematic diagram of randomly extracted and uniformly extracted impedance matrix.

Because $\mathbf{I}$ is not sparse, a sparse transformation of $\mathbf{I}$ is performed to satisfy the CS framework as follows:

$$\mathbf{I} = \mathbf{\Psi}\alpha, \tag{5}$$

where $\boldsymbol{\alpha}$ is the vector of weight coefficients, and $\mathbf{\Psi}$ is the sparse basis. Thus, (4) transforms as:

$$\tilde{\mathbf{Z}}I = \tilde{\mathbf{Z}}\mathbf{\Psi}\boldsymbol{\alpha} = \mathbf{\Theta}\boldsymbol{\alpha} = \tilde{\mathbf{V}}, \tag{6}$$

where $\mathbf{\Theta}$ is the sensing matrix. Typically, to ensure that (6) can be solved with high probability, the sensing matrix $\mathbf{\Theta}$ requires to satisfy the restricted isometry property (RIP) [26]:

$$1 - \omega \leq \frac{\|\mathbf{\Theta}\boldsymbol{\alpha}\|_2^2}{\|\boldsymbol{\alpha}\|_2^2} \leq 1 + \omega, \tag{7}$$

where constant $\omega \in (0, 1)$. However, the proofs and applications of RIP are relatively abstract, posing significant challenges in theory and practice. For this reason, Baraniuk proposed a more intuitive equivalent condition [27]: the incoherence between the measurement matrix $\tilde{\mathbf{Z}}$ and the sparse basis $\mathbf{\Psi}$. In simple terms, it means that the rows of the measurement matrix and the columns of the sparse basis cannot represent each other.

To obtain the recovery value, greedy algorithms such as orthogonal matching pursuit (OMP) [28] or generalized OMP

(gOMP) [29] are commonly used as recovery algorithms to solve (6).

2.2. The Sparse Basis Construction

Consider that CMs are generated independently of the excitations and solved efficiently, and [15] also demonstrates that CMs are more advantageous than CBFs. Thus, CMs are used as sparse basis to achieve the sparse transformation of currents. According to the CM theory of PEC, CMs are obtained by solving the generalized eigenvalue equation [30]. To accelerate the solution of CMs, the object is divided into m blocks, and the impedance matrix $\mathbf{Z}$ is transformed into the following form:

$$\mathbf{Z} = \begin{bmatrix} \mathbf{Z}_{11} & \mathbf{Z}_{12} & \dots & \mathbf{Z}_{1m} \\ \mathbf{Z}_{21} & \mathbf{Z}_{22} & \dots & \mathbf{Z}_{2m} \\ \vdots & \vdots & \ddots & \vdots \\ \mathbf{Z}_{m1} & \mathbf{Z}_{m2} & \dots & \mathbf{Z}_{mm} \end{bmatrix}, \tag{8}$$

where $\mathbf{Z}_{ii}$ and $\mathbf{Z}_{ij}$ $(i, j = 1, 2, \dots, m)$ denote the self-impedance matrix and mutual impedance matrix, respectively. Meanwhile, each block extends 0.15 wavelength outward to ensure the continuity of the current. Afterwards, the CMs for each block are generated from the generalized eigenvalue equation formed by the self-impedance matrix:

$$\mathbf{X}_{ii}^{e}\mathbf{J}_{i}^{e} = \lambda_i \mathbf{R}_{ii}^{e}\mathbf{J}_{i}^{e}, \tag{9}$$

in which, $\mathbf{Z}_{ii}^{e} = \mathbf{R}_{ii}^{e} + j\mathbf{X}_{ii}^{e}$. λ_i and $\mathbf{J}_{i}^{e}$ represent the eigenvalue and their corresponding CM. e indicates extension. Then, low-order CMs are selected by modal significance (MS):

$$MS = \left| \frac{1}{1 + j\lambda_i} \right|. \tag{10}$$

A threshold τ is set, and the CMs corresponding to the eigenvalues that satisfy the condition $MS > \tau$ are low-order CMs. Finally, the sparse basis $\mathbf{\Psi}$ is formed after removing the extensions in these CMs.

2.3. ACA-CS-MoM

In the MoM, the RWG basis function is used as basis function combined with the Galerkin method to construct the impedance matrix $\mathbf{Z}$. Thus, (1) can be transformed into the following form:

$$\mathbf{Z} = \begin{bmatrix} \langle w_1, L(f_1)\rangle & \langle w_1, L(f_2)\rangle & \dots & \langle w_1, L(f_N)\rangle \\ \langle w_2, L(f_1)\rangle & \langle w_2, L(f_2)\rangle & \dots & \langle w_2, L(f_N)\rangle \\ \vdots & \vdots & \ddots & \vdots \\ \langle w_N, L(f_1)\rangle & \langle w_N, L(f_2)\rangle & \dots & \langle w_N, L(f_N)\rangle \end{bmatrix}, \tag{11}$$

$$\mathbf{V} = \begin{bmatrix} \langle w_1, g\rangle \\ \langle w_2, g\rangle \\ \vdots \\ \langle w_N, g\rangle \end{bmatrix}, \tag{12}$$

where $(w_m = f_m)$ denotes the test function. $L(\cdot)$ and g represent linear operator and known excitation source, respectively. Obviously, the test function corresponds to each row of $\mathbf{Z}$ respectively, and each test function contains distinct spatial distribution information, resulting in different impacts on the computational results. In other words, different test functions contribute differently to the accuracy. Therefore, in CS-MoM, the participation of measurement matrix constructed from different rows in the computation leads to different results.

In previous CS model, it was common to randomly extract certain rows of the impedance matrix to use as measurement matrix. But this randomization strategy results in unstable calculations. Likewise, NCS-MoM [16] constructs the measurement matrix by uniformly extracting the impedance matrix and obtains stable computational results, but it is still a simple extraction method. Although more test functions can achieve higher accuracy, extracting the rows corresponding to test functions that contribute higher can also generate satisfied results. Evidently, random extraction and uniform extraction are hardly guaranteed to find these highly contributive test functions, especially at low extraction ratios. In contrast, the ACA algorithm, based on weight scheme and independent of Green's functions, can recognize the rows and columns with significant influence within the matrix. Therefore, the proposed method introduces ACA to recognize the rows corresponding to these test functions.

To begin with, we divide the objects into blocks and then set a control parameter δ to split the impedance matrix into near-field and far-field groups. Once the condition $C_d >= 0.05\lambda$ and $C_d >= \delta b_s$ is met, ACA processing is performed to compress $\mathbf{Z}_{ij}$, where λ denotes the wavelength, and C_d and b_s are the center distance between two blocks and the block size, respectively.

The purpose of ACA is to approximate $\mathbf{Z}_{ij}$ by transforming it into a product of two matrixes, namely:

$$\mathbf{Z}_{ij}^{a\times b} \approx \mathbf{U}^{a\times r} \cdot \mathbf{V}^{r\times b}, \tag{13}$$

where $\mathbf{U}^{a\times r}$ and $\mathbf{V}^{r\times b}$ are two rectangular matrixes, and r is the effective rank of the matrix $Z_{ij}^{a\times b}$, which is also the number of rows and columns recognized by ACA. The major procedure of the ACA algorithm is given in Algorithm 1. In Algorithm 1, r_i is the row index we need. $\mathbf{u}_k$ and $\mathbf{v}_k$denote the kth column of $\mathbf{U}^{a\times r}$ and the kth row of $\mathbf{V}^{r\times b}$, respectively. It should be noted that unlike the traditional ACA used to accelerate the MVPs, this method involves only r_i in the subsequent computation.

Algorithm 1 Procedure Index generation

for $i = 1, 2, 3, \dots, m$ **do**
Set $max\_num = 0$
for $j = 1, 2, 3, \dots, m$ **do**
if $\mathbf{Z}_{ij}$ compliance with ACA **do**
Obtain r_j
if $r_j \geq max\_num$ **do**
Let $max\_num = r_j$
end if
end if
end for
Let $r_i = max\_num$
end for

Algorithm 2 gOMP

Input:	sensing matrix $\boldsymbol{\Theta}$ measurement value $\tilde{\mathbf{V}}$, sparsity K number of indexes for each selection S.
Initialize:	iteration count k residual vector $\mathbf{r}^0 = \tilde{\mathbf{V}}$, estimated support set $\Lambda_0 = \emptyset$.
1:	**while** $k < K$ and $\left\|\mathbf{r}^k\right\|_2 > \sigma\ (\sigma > 0)$ **do**
2:	$k = k + 1$;
3:	Select indexes $\phi_1, \phi_2, \ldots, \phi_S$ corresponding to S largest entries in $\boldsymbol{\Theta}^T \mathbf{r}^{k-1}$;
4:	$\Lambda_k = \Lambda_{k-1} \cup \{\phi_1, \phi_2, \ldots, \phi_S\}$;
5:	$\hat{\alpha}_{\Lambda_k} = \arg\min_u \left\|\tilde{\mathbf{V}} - \boldsymbol{\Theta}_{\Lambda_k} u\right\|_2 = \left(\boldsymbol{\Theta}_{\Lambda_k}^T \boldsymbol{\Theta}_{\Lambda_k}\right)^{-1} \left(\boldsymbol{\Theta}_{\Lambda_k}^T \tilde{\mathbf{V}}\right)$;
6:	$\mathbf{r}^k = \tilde{\mathbf{V}} - \boldsymbol{\Theta}_{\Lambda_k} \hat{\alpha}_{\Lambda_k}$;
7:	**end while**
Output:	$\alpha = \hat{\alpha}$.

Specifically, if there is a matrix that satisfies the condition C_d, it is subjected to ACA compression, and the row indexes generated during the process are recorded. As for the $\mathbf{U}^{a\times r}$ and $\mathbf{V}^{r\times b}$ matrix, it will not be involved in the subsequent vector product operations.

As shown in Figure 2, ACA is utilized to recognize far-field groups, and a set of row indexes is obtained, corresponding to the test functions. However, the dimension of each far-field group is different, resulting in varying number of test functions recognized by ACA. To ensure accuracy, we select the far-field group that recognizes more test functions and output the row indexes corresponding to the test functions. For example, in far-field groups $\mathbf{Z}_{03}$ to $\mathbf{Z}_{07}$ in Figure 2, if $\mathbf{Z}_{03}$ recognizes the highest number of test functions, the row indexes corresponding to the test functions therein are output. This is because each far-field group definitely contains the same test functions, and selecting the far-field group that recognizes the higher number of test functions maximizes the retention of test functions that contribute significantly to accuracy. Therefore, following this approach, a set of deterministic row indexes can be obtained.

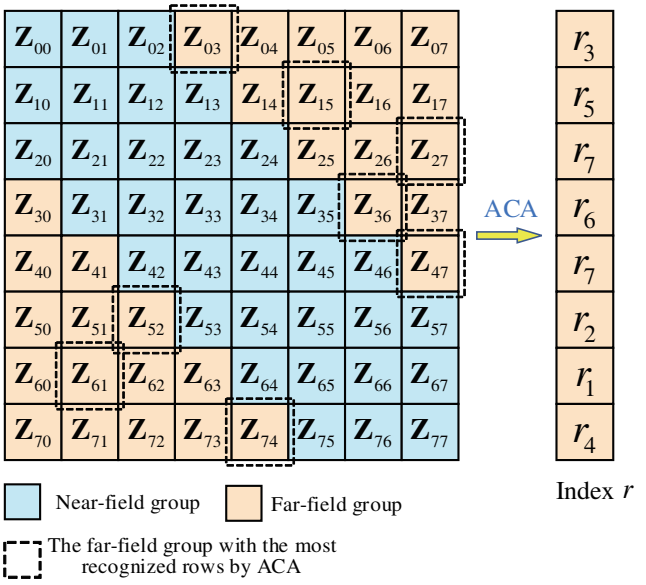

FIGURE 2. The process of recognizing significant rows in the matrix using ACA.

Subsequently, a determined measurement matrix can be obtained by extracting the impedance matrix according to these row indexes correspondingly. In addition, different ACA thresholds recognize varying number of test functions, resulting in different dimensions of the constructed measurement matrixes. Similar to NCS-MoM, which controls the accuracy by adjusting the extraction step size, the proposed method achieves the effect of controlling the accuracy by changing the dimension of the measurement matrix through adjusting the threshold of ACA. However, the step size of uniform extraction in NCS-MoM is integer, making it difficult to control the number of extracted rows. It is worth mentioning that the proposed method avoids generating unstable computational results and enables finely adjusted number of extracted rows, which possesses the advantages of both random extraction and uniform extraction.

To facilitate comparison, the CMs are adopted as the sparse basis to establish the overdetermined equation. However, using the greedy algorithm to reconstruct the current coefficients tends to pursue local optimality, leading to lose sight of the overall accuracy. Although gOMP improves accuracy by increasing the sampling rate without increasing the sampling time, the identification process for the sensing matrix remains time-consuming. The procedure of gOMP is shown in Algorithm 2. Because the columns to be recognized in sensing matrix $\boldsymbol{\Theta}$ correspond to the sparse basis (CMs), it is possible to skip the recognition process and directly use least squares to obtain the coefficient vector instead of iterative solving. The form of the least squares solution is as follows. Substituting (14) to (5), the approximate current $\mathbf{I}$ is obtained.

$$\boldsymbol{\alpha} = \left(\boldsymbol{\Theta}^T \boldsymbol{\Theta}\right)^{-1} \left(\boldsymbol{\Theta}^T \tilde{\mathbf{V}}\right). \tag{14}$$

Compared to recent methods CS-CMs [15] and NCS-MoM [16], the proposed method ACA-CS-MoM employs ACA to recognize crucial rows within the impedance matrix for constructing the measurement matrix. While ensuring stability and accuracy, the proposed method improves computational efficiency due to the smaller dimension of the constructed measurement matrix.

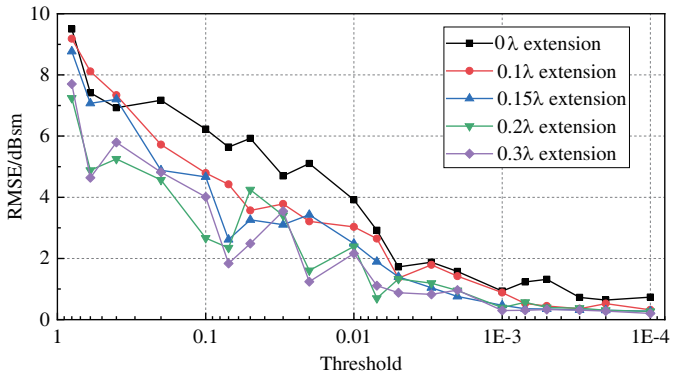

FIGURE 3. Variation of errors with threshold under different extension sizes.

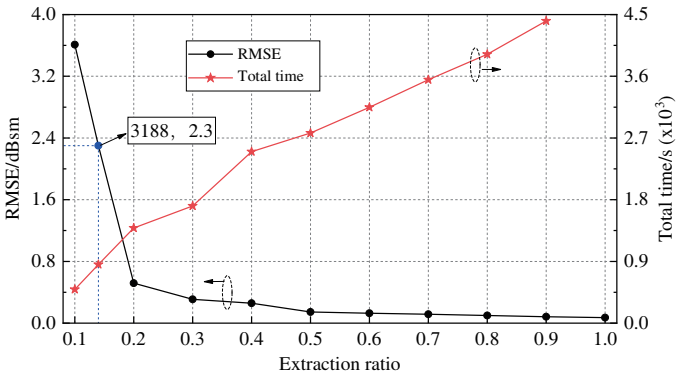

FIGURE 4. Calculation errors and time for CS-CMs under random extraction.

3. COMPLEXITY ANALYSIS

In this section, the comparisons of CS-CMs, NCS-MoM, and ACA-CS-MoM are performed in terms of the measurement matrix construction, the sparse basis generation, and the current reconstruction. For the sake of comparison, it is assumed that the unknowns in each block are equal, and the number of extracted rows is controlled to be the same for both CS-CMs and NCS-MoM.

(1) Measurement matrix construction: Suppose that the number of rows extracted by CS-CMs and NCS-MoM is M, and the number of rows extracted by ACA-CS-MoM is P. Thus, the complexity of the former is $O(MN)$. For ACA-CS-MoM, this portion also contains the time that the ACA calculates indexes, then its complexity is:

$$O\left(\frac{1}{2}m^2r\left(\frac{N}{m}+\frac{N}{m}\right)+PN\right) = O\left((mr+P)N\right)\approx O(PN), \tag{15}$$

since P is commonly much smaller than M, the complexity of ACA-CS-MoM in this process is much lower.

(2) Sparse basis generation: In this step, the main solution is to solve (9) by LU factorization, and its complexity is:

$$O\left(m\left(\frac{N}{m}\right)^3\right) = O\left(\frac{1}{m^2}N^3\right). \tag{16}$$

(3) Current reconstruction: This step primarily consists of constructing the sensing matrix $\boldsymbol{\Theta}$ and solving (6). Assuming that the total number of CMs is K, the complexity of CS-CMs is:

$$O(MNK+SMK) = O\left(K(MN+SM)\right). \tag{17}$$

In contrast, the computational complexity of ACA-CS-MoM is:

$$O(PNK+PK) = O\left(K(PN+P)\right). \tag{18}$$

Clearly, ACA-CS-MoM has the lowest complexity in this process. In summary, compared to CS-CMs and NCS-MoM, the proposed method ACA-CS-CMs has lower computational complexity and significantly improves the computational efficiency.

4. NUMERICAL RESULTS

To test the effectiveness of the proposed method, different objects are simulated and analyzed. The root mean square error (RMSE) is used to evaluate the accuracy of calculating the radar cross section (RCS) by different methods, denoted as:

$$RMSE = \sqrt{\frac{1}{N_a}\sum_{i=1}^{N_a}\left(\sigma_{cal}-\sigma_{MoM}\right)^2}, \tag{19}$$

where N_a is the sample number, and σ_{cal} and σ_{MoM} denote the calculation results of the method used and MoM, respectively. In addition, in all simulations, the number of rows extracted in the impedance matrix is controlled to be equal for CS-CMs and NCS-MoM.

First, the bistatic RCS of a perfect electric conductor (PEC) cylinder with a radius of 0.2 m and a height of 1 m at the incident frequency of 1.5 GHz is analyzed. The surface of the cylinder is discretized into 15,184 triangular patches and 22,776 unknowns. Meanwhile, the cylinder is divided into 16 blocks. The threshold τ of MS is set to 0.0002, and each block is extended by 0.15λ, obtaining 1915 CMs and 35,564 unknowns.

The variation of errors with threshold under different extension sizes is given in Figure 3. It can be observed that the overall trend of the error is reduced as τ decreases. Meanwhile, as the extension size increases, the computational accuracy improves, but the computational time increases accordingly. To balance time and accuracy, the extended size and τ are set to 0.15λ and 0.0002, respectively.

Subsequently, the variations in accuracy and computation time for CS-CMs, NCS-MoM, and ACA-CS-MoM under different influencing factors are demonstrated in Figure 4, Figure 5, and Figure 6, respectively. It is clearly found that among the three extraction strategies, extracting more rows to construct the measurement matrix leads to higher accuracy. The reason is that more test functions are involved in the testing procedure. However, as the number of extracted rows increases, the time cost gradually grows. The blue points in Figure 4, Figure 5, and Figure 6 show that the RMSE is 2.3 when rows 3188 are extracted randomly, 0.64 when rows 3253 are extracted uniformly, and 0.3 when rows 3129 are extracted using ACA. Therefore, to balance the time and accuracy, the extraction step

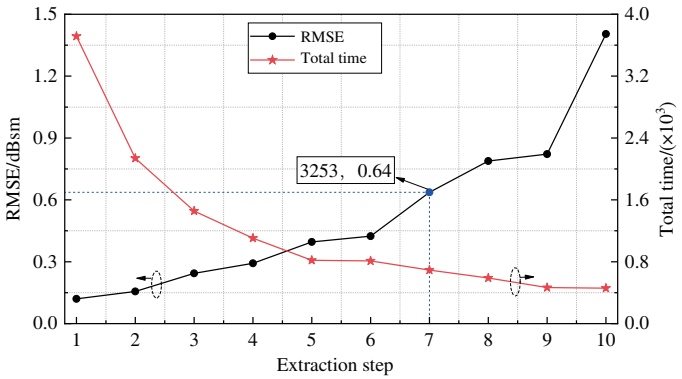

FIGURE 5. Calculation errors and time for NCS-MoM under uniform extraction.

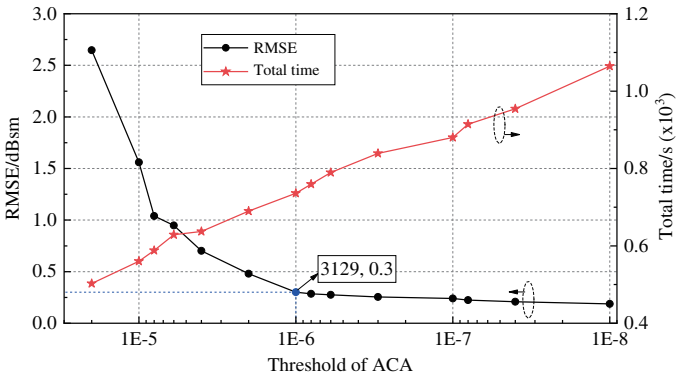

FIGURE 6. Calculation errors and time for ACA-CS-MoM under different thresholds.

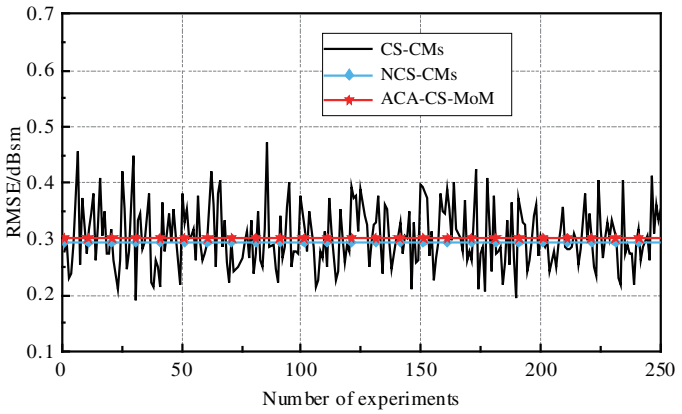

FIGURE 7. Calculation errors and time for ACA-CS-MoM under different thresholds.

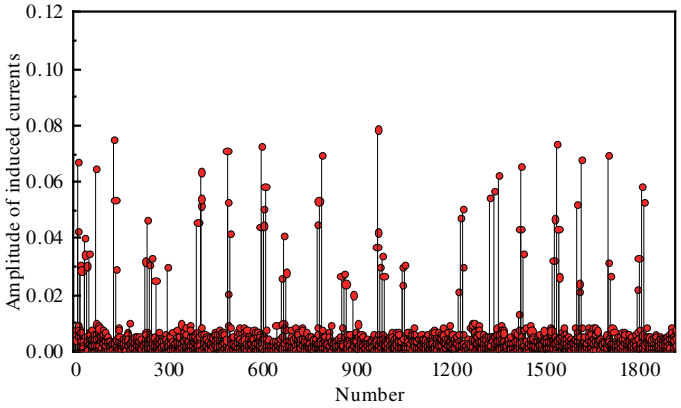

FIGURE 8. Amplitude of the induced currents on the sparse basis.

size and the threshold of the ACA are set to 4 and 1E-6, respectively.

Our aim is to make the dimension of the measurement matrix constructed by CS-CMs and NCS-MoM consistent.

The number of rows extracted for CS-CMs is equal to that of NCS-MoM, and its extraction ratio is set to 0.25. Based on this, 250 experiments are conducted for the three methods, and the computational results are shown in Figure 7. Obviously, the error of CS-CMs fluctuates between 0.2 and 0.5, while NCS-MoM and ACA-CS-MoM are capable of ensuring the stability of the computational results. In addition, Figure 8 illustrates the sparsity of induced currents on the sparse basis constructed by CMs. The amplitude of the induced currents on the sparse basis is mostly close to zero, with a few elements dominating and displaying fine sparsity.

To confirm the reasonableness of ACA-CS-MoM, the correlation coefficients [12] between the measurement matrix and the sparse basis under three extraction strategies are compared shown in Table 1. The correlation coefficient is calculated as:

$$\mu\left(\boldsymbol{\Theta}\right) = \max_{i \neq j} \frac{|\theta_i^* \theta_j|}{\|\theta_i\| \cdot \|\theta_j\|}, \tag{20}$$

where θ_i and θ_j are the ith and jth columns in $\boldsymbol{\Theta}$, respectively. As can be seen in Table 1, the correlation coefficients calculated under three extraction strategies are close to zero, which indicates that the proposed method is feasible.

TABLE 1. Correlation coefficient between the measurement matrix and the sparse basis.

Method	Extracting strategy	μ
CS-CMs	Random extraction	0.0133
NCS-MoM	Uniform extraction	0.0141
ACA-CS-MoM	The row index of ACA	0.0138

Eventually, the dimensions of the measurement matrixes constructed by CS-CMs and NCS-MoM are both 5694×22776. Under the condition of similar accuracy, the dimension of the measurement matrix constructed by ACA-CS-MoM is 3129×22776. It is clearly found that the dimension of the measurement matrix in the proposed method is lower making the reconstruction of the current become more efficient. In addition, the bistatic RCS results of the cylinder in vertical polarization are given in Figure 9. The computational results demonstrate a high accuracy of the proposed method.

Next, the bistatic RCS of a PEC almond with the length of 504.748 mm is considered. The incident frequency is 4 GHz, and the surface of the almond is discretized into 39,186 triangular patches by the RWG basis function, generating 58,779

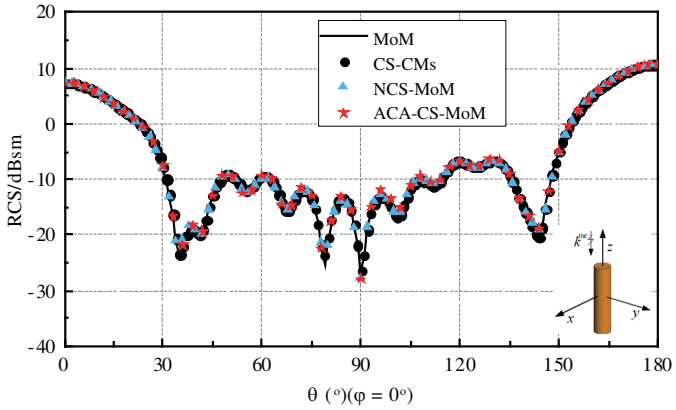

FIGURE 9. The bistatic RCS results of the cylinder in vertical polarization.

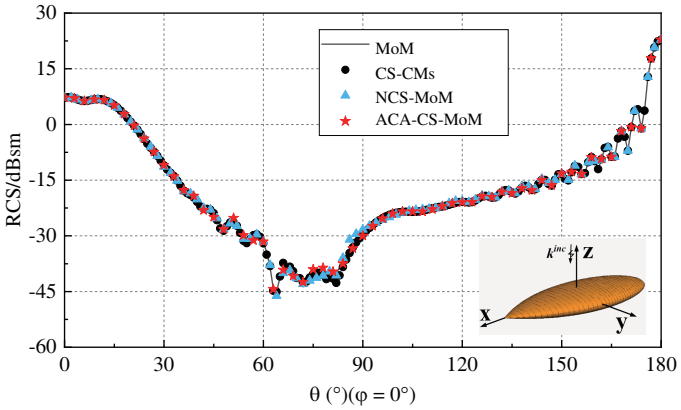

FIGURE 10. The bistatic RCS results of the almond in vertical polarization.

TABLE 2. Simulation time for different processes.

Model	Method	Time to calculate indexes (s)	Number of rows extracted	Constructing measurement matrix time (s)	Solving time (s)	Total time (s)	RMSE (dBsm)	Memory of measurement matrix (GB)
Cylinder	CS-CMs		5694	606.8	430.1	1235.4	0.34	1.93
	NCS-MoM		5694	603.9	325.6	1104.7	0.29	1.93
	ACA-CS-MoM	71.5	3129	324.2	168.3	736.1	0.30	1.06
Almond	CS-CMs		19593	5862.1	17246.0	23708.6	0.41	17.12
	NCS-MoM		19593	5863.7	12177.9	18671.1	0.53	17.12
	ACA-CS-MoM	969.1	12410	3565.9	7240.1	12271.2	0.47	10.86
Cone-sphere with gap	CS-CMs		26226	10133.3	37234.4	48726.2	0.19	30.74
	NCS-MoM		26226	10128.5	28221.6	39520.3	0.19	30.74
	ACA-CS-MoM	1599.0	18798	6823.2	19197.2	28864.9	0.21	22.03

unknowns. Then, the object is divided into 36 blocks, and each block is extended by 0.15 wavelength to yield 105,181 unknowns. The threshold of MS is set to 0.0002, resulting in 5675 CMs. Afterwards, the extraction ratio and extraction step for CS-CMs and NCS-MoM are set to 1/3 and 3, respectively, and the dimensions of the constructed measurement matrixes are both 19593×58779. Under comparable accuracy conditions, the threshold for ACA in ACA-CS-MoM is set to 1E-8, yielding a measurement matrix dimension of 12410×58779. Moreover, the calculation of bistatic RCS for vertical polarization of almond using different methods is illustrated in Figure 10. The computational results indicate that the proposed method has excellent computational accuracy.

Finally, the bistatic RCS of a PEC cone-sphere with gap, approximately 0.7 m in length, is calculated at an incident frequency of 8 GHz. The surface of the object is discretized to form 52,452 triangular patches and 78,678 unknowns. The threshold of MS is set to 0.0002. Subsequently, the object is divided into 56 blocks, and each block is extended separately by 0.15λ, which generates 7690 CMs and 149,319 unknowns. Moreover, the extraction ratio and extraction step for CS-CMs and NCS-MoM are set to 1/3 and 3, respectively, and the dimensions of the constructed measurement matrices are both 26226×78678. In the case of similar accuracy, the threshold of ACA is 1E-8 in ACA-CS-MoM, and the dimension of the constructed measurement matrix is 18798×78678. In contrast, the proposed method extracts fewer rows, resulting in higher computational efficiency. Meanwhile, the bistatic RCS results of cone-sphere with gap are shown in Figure 11. Obviously, the calculated results of the proposed method are in excellent agreement with the MoM.

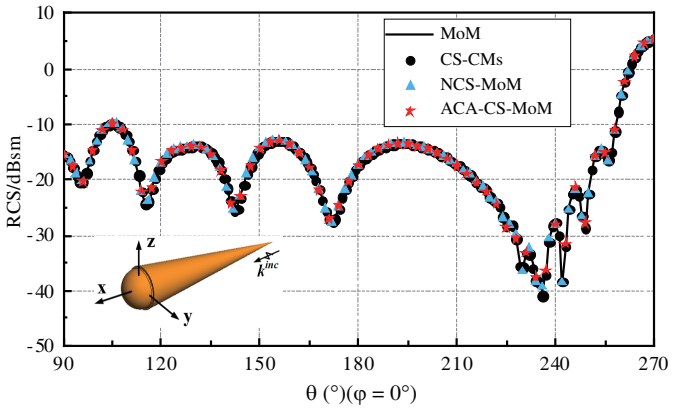

FIGURE 11. The bistatic RCS results of the cone-sphere with gap in vertical polarization.

The simulation times of different processes corresponding to Figure 9, Figure 10, and Figure 11 are given in Table 2. Note that CS-CMs and NCS-MoM use gOMP and the least squares method for current recovery, respectively. Therefore, these two methods are different in terms of solution time and RMSE. Clearly, the proposed method extracts fewer rows while ensuring accuracy, resulting in a significant reduction in the construction time of the measurement matrix, as well as the time for solving the overdetermined equation. Although ACA-CS-MoM requires additional time to recognize the row indexes corresponding to the test functions in advance when constructing the measurement matrix, this time is relatively small compared to the overall reduction in computation time. From the point of view of computing memory for the measurement matrix, the new method reduces 45%, 36%, and 26% in three instances, respectively. The accuracy and efficiency of the proposed method are demonstrated through the above numerical simulation analysis.

5. CONCLUSION

In this paper, a novel scheme is proposed to improve the performance of CS-MoM. By introducing ACA to recognize the significant test functions in the impedance matrix, the impedance matrix is extracted based on its row indexes correspondingly to construct the measurement matrix. Higher accuracy is achieved with fewer observations. Meanwhile, the least squares is employed as the recovery algorithm to achieve efficient reconstruction of the induced currents. Theoretical and simulation analyses demonstrate that, in comparison to CS-CMs and NCS-MoM, the proposed ACA-CS-MoM reduces the computation time while ensuring the computational accuracy.

ACKNOWLEDGEMENT

This work was supported in part by the Natural Science Foundation of Anhui Provincial Education Department under Grant no. 2022AH051583 and No. 2022AH052138, in part by the National Natural Science Foundation of China under Grant No. 62071004 and No. 61401003, in part by the Anhui Province Graduate Academic Innovation Project under grant No. 2023xscx074.

REFERENCES

[1] Harrington, R. F., "Field computation by moment methods," *The Macmillan Comp.*, Vol. 130, No. 6, 276–280, 1968.

[2] Gibson, W. C., *The Method of Moments in Electromagnetics*, 2007.

[3] Coifman, R., V. Rokhlin, and S. Wandzura, "The fast multipole method for the wave equation: A pedestrian prescription," *IEEE Antennas and Propagation Magazine*, Vol. 35, No. 3, 7–12, 1993.

[4] Song, J., C.-C. Lu, and W. C. Chew, "Multilevel fast multipole algorithm for electromagnetic scattering by large complex objects," *IEEE Transactions on Antennas and Propagation*, Vol. 45, No. 10, 1488–1493, 1997.

[5] Prakash, V. V. S. and R. a. Mittra, "Characteristic basis function method: A new technique for efficient solution of method of moments matrix equations," *Microwave and Optical Technology Letters*, Vol. 36, No. 2, 95–100, 2003.

[6] Garcia, E., C. Delgado, I. G. Diego, and M. F. Catedra, "An iterative solution for electrically large problems combining the characteristic basis function method and the multilevel fast multipole algorithm," *IEEE Transactions on Antennas and Propagation*, Vol. 56, No. 8, 2363–2371, 2008.

[7] Donoho, D. L., "Compressed sensing," *IEEE Transactions on Information Theory*, Vol. 52, No. 4, 1289–1306, 2006.

[8] Candes, E. J., J. Romberg, and T. Tao, "Robust uncertainty principles: Exact signal reconstruction from highly incomplete frequency information," *IEEE Transactions on Information Theory*, Vol. 52, No. 2, 489–509, 2006.

[9] Kong, M., M. Chen, X. Cao, L. Zhang, Q. Qi, and X. Wu, "Fast analysis of local current distribution for electromagnetic scattering problems of electrically large objects," *IEEE Access*, Vol. 8, 127 640–127 647, 2020.

[10] Kong, M., M. S. Chen, X. Y. Cao, J. B. Zhu, X. J. Kuang, Q. Qi, and X. L. Wu, "Fast electromagnetic scattering analysis of inhomogeneous dielectric objects over a wide incident angle," *IEEE Antennas and Wireless Propagation Letters*, Vol. 20, No. 8, 1527–1531, 2021.

[11] Chai, S.-R. and L.-X. Guo, "Compressive sensing for monostatic scattering from 3-D NURBS geometries," *IEEE Transactions on Antennas and Propagation*, Vol. 64, No. 8, 3545–3553, 2016.

[12] Chai, S.-R. and L.-X. Guo, "Integration of CS into MoM for efficiently solving of bistatic scattering problems," *IEEE Antennas and Wireless Propagation Letters*, Vol. 15, 1771–1774, 2016.

[13] Wang, Z., B.-Z. Wang, and W. Shao, "Efficient construction and solution of MoM matrix equation with compressed sensing technique," *Journal of Electromagnetic Waves and Applications*, Vol. 29, No. 5, 683–692, 2015.

[14] Chai, S.-R. and L.-X. Guo, "Fast analysis of bistatic scattering problems with compressive sensing technique," *Journal of Electromagnetic Waves and Applications*, Vol. 30, No. 13, 1755–1762, 2016.

[15] Wang, Z., P. Wang, Y. Sun, and W. Nie, "Fast analysis of bistatic scattering problems for three-dimensional objects using compressive sensing and characteristic modes," *IEEE Antennas and Wireless Propagation Letters*, Vol. 21, No. 9, 1817–1821, 2022.

[16] Gao, Y., M. F. Akbar, and G. N. Jawad, "Stabilized and fast method for compressive sensing-based method of moments," *IEEE Antennas and Wireless Propagation Letters*, Vol. 22, No. 12, 2915–2919, 2023.

[17] Rao, S., D. Wilton, and A. Glisson, "Electromagnetic scattering by surfaces of arbitrary shape," *IEEE Transactions on Antennas and Propagation*, Vol. 30, No. 3, 409–418, 1982.

[18] Wang, Z.-G., W.-Y. Nie, and H. Lin, "Characteristic basis functions enhanced compressive sensing for solving the bistatic scattering problems of three-dimensional targets," *Microwave and Optical Technology Letters*, Vol. 62, No. 10, 3132–3138, 2020.

[19] Wang, P., Z.-G. Wang, Y.-F. Sun, and W.-Y. Nie, "Novel compressive sensing computing model used for analyzing electromagnetic scattering characteristics of three-dimensional electrically large objects," *Acta Physica Sinica*, Vol. 72, No. 3, 54–61, 2023.

[20] Chen, Y. and C.-F. Wang, *Characteristic Modes: Theory and Applications in Antenna Engineering*, John Wiley & Sons, 2015.

[21] Cao, X., M. Chen, Q. Qi, M. Kong, J. Hu, L. Zhang, and X. Wu, "Solving electromagnetic scattering problems by underdetermined equations and Krylov subspace," *IEEE Microwave and Wireless Components Letters*, Vol. 30, No. 6, 541–544, 2020.

[22] Wang, Z., H. Yuan, Y. Sun, W. Nie, and P. Wang, "Block-based krylov subspace basis functions for solving bistatic scattering problems," *IEEE Antennas and Wireless Propagation Letters*, Vol. 22, No. 10, 2561–2565, 2023.

[23] Kurz, S., O. Rain, and S. Rjasanow, "The adaptive cross-approximation technique for the 3D boundary-element method," *IEEE Transactions on Magnetics*, Vol. 38, No. 2, 421–424, 2002.

[24] Zhao, K., M. N. Vouvakis, and J.-F. Lee, "The adaptive cross approximation algorithm for accelerated method of moments computations of EMC problems," *IEEE Transactions on Electromagnetic Compatibility*, Vol. 47, No. 4, 763–773, 2005.

[25] Lloyd, S., "Least squares quantization in PCM," *IEEE Transactions on Information Theory*, Vol. 28, No. 2, 129–137, 1982.

[26] Candès, E. J., "The restricted isometry property and its implications for compressed sensing," *Comptes Rendus. Mathematique*, Vol. 346, No. 9-10, 589–592, 2008.

[27] Baraniuk, R. G., "Compressive sensing," *IEEE Signal Process. Mag.*, Vol. 24, No. 4, 118–121, 2007.

[28] Tropp, J. A. and A. C. Gilbert, "Signal recovery from random measurements via orthogonal matching pursuit," *IEEE Transactions on Information Theory*, Vol. 53, No. 12, 4655–4666, 2007.

[29] Wang, J., S. Kwon, and B. Shim, "Generalized orthogonal matching pursuit," *IEEE Transactions on Signal Processing*, Vol. 60, No. 12, 6202–6216, 2012.

[30] Harrington, R. and J. Mautz, "Theory of characteristic modes for conducting bodies," *IEEE Transactions on Antennas and Propagation*, Vol. 19, No. 5, 622–628, 1971.